Supplement of Atmos. Chem. Phys., 26, 5375–5406, 2026
https://doi.org/10.5194/acp-26-5375-2026-supplement

Atmospheric Chemistry and Physics
Open Access
EGU

Supplement of

Global atmospheric methanol emissions inferred from IASI satellite measurements and aircraft data

Jean-François Müller et al.

Correspondence to: Jean-François Müller (jfm@aeronomie.be)

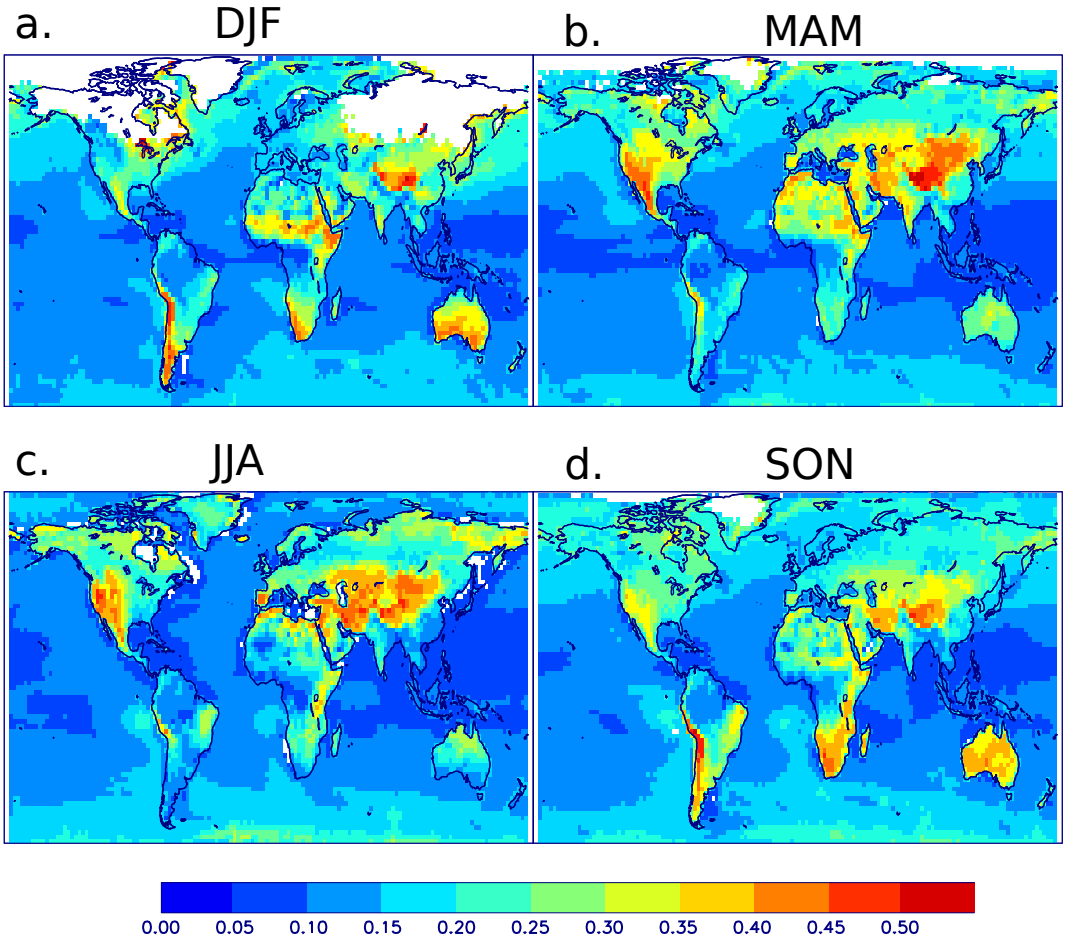

Figure S1. Seasonally-averaged distribution of the IASI total column averaging kernel at the first IASI grid layer (0–0.14 km altitude). Average over 2008–2019.

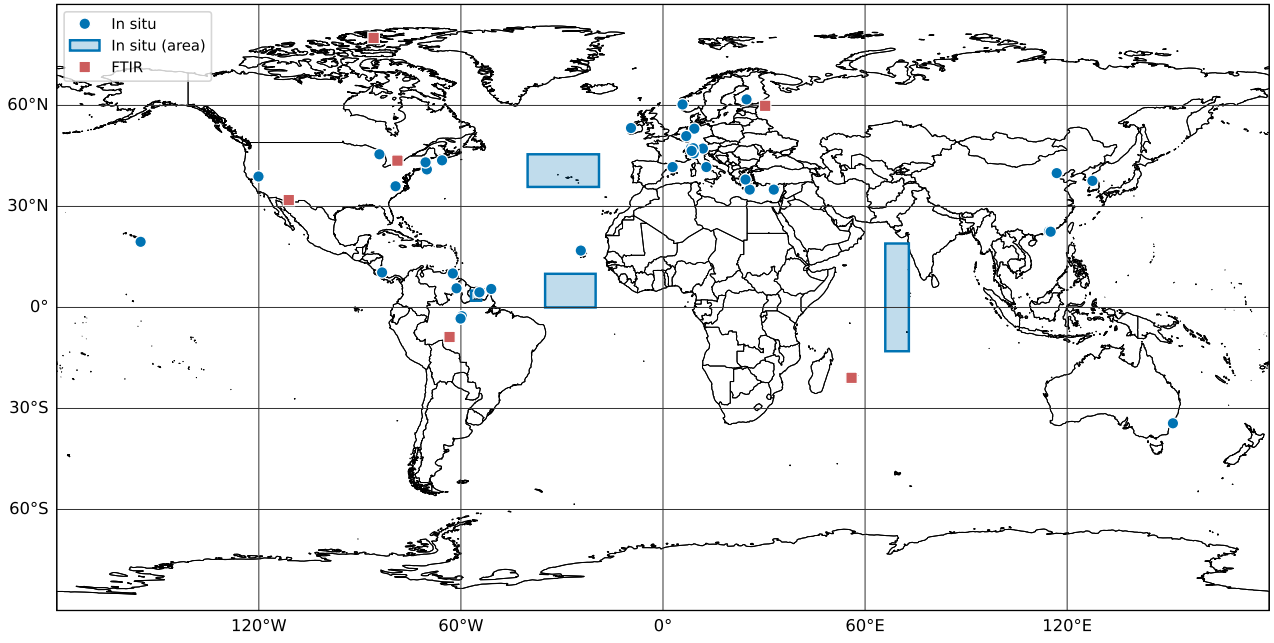

Figure S2. Location of in situ CH_3OH measurement sites used for model evaluation (blue dots and blue boxes), presented in Tables S1 and S2. Red squares correspond to the location of FTIR measurement sites, Eureka (80.05 N, 273.58 E), Saint Petersburg (59.88 N, 29.83 E), Toronto (43.6 N, 280.64 E), Jungfraujoch (46.55 N, 7.98 E), Kitt Peak (31.9 N, 248.4 E), Porto Velho (8.77 S, 296.13 E), Saint-Denis, Reunion Isl. (20.90 S, 55.49 E), and Maïdo Observatory, Reunion Isl. (21.08 S, 55.38 E).

Table S1. In situ CH_3OH mixing ratio measurements (pptv), and corresponding model values from the a priori run and IASI-based inversion. Obs.: average from observation. A priori and optimised model values are averages calculated for the year and months of the measurement campaign when simulations are available for that year, otherwise a climatology is calculated using all simulated years (2008-2019).

Site	Coordinates	Month	Obs.	A priori	Optimised	Reference
		Tropical forests				
Malaysian rainforest (2008)	5.0 N, 117.8 E	4-5	1200	2797	1396	Langford et al. (2010)
Malaysian rainforest (2008)	5.0 N, 117.8 E	6-7	1500	2314	1481	Langford et al. (2010)
Suriname trop. forest (2005)	4.5 N, 305.0 E	10	1890	2615	1773	Lelieveld et al. (2008)
Rondonia, Brazil (1999)	10.1 S, 297.1 E	10	2500	5164	5962	Kesselmeier et al. (2002)
Suriname rainforest (1998)	2-5 N, 303-306 E	3	1100	1782	1263	Williams et al. (2001)
Central Amazonia (2004)	2.6 S, 299.8 E	9	4100	5700	4738	Karl et al. (2007)
Parupa, Venezuela (1999)	5.7 N, 298.2 E	1-2	1540	2053	1397	Sanhueza et al. (2001)
La Selva, Costa Rica (2003)	10.4 N, 276.1 E	4-5	2155	1912	1467	Karl et al. (2004)
Manacapuru, Brazil (2014)	3.3 S, 299.4 E	2	1778	3015	2148	Seco et al. (2014)
Manacapuru, Brazil (2014)	id.	3	1261	3197	2447	Seco et al. (2014)
		North America				
Blodgett Forest, USA (2000)	38.9 N, 239.4 E	6	3650	2557	3880	Schade and Goldstein (2006)
id.	id.	9-11	3440	1632	2073	id.
id.	id.	12-1	970	985	1145	id.
id. (2001)	id.	3	1900	1268	1929	id.
Appledore Isl., USA (2004)	41 N, 289.4 E	7-8	2100	3129	3900	Mao et al. (2006)
Duke Forest, USA (2003)	36 N, 280.1 E	7	5000	6854	7184	Karl et al. (2005)
Chebogue Point, Canada (2004)	43.7 N, 293.9 E	7-8	1389	2134	3281	Millet et al. (2006)
UMBS, Michigan, USA (2001)	45.5 N, 275.3 E	9-10	3530	1359	2233	Karl et al. (2003)
UMBS, Michigan, USA (2002)	id.	6	6800	4046	6343	id.
UMBS, Michigan, USA (2005)	id.	7-8	8050	3732	5853	id.
Durham, USA (2005-2007)	43.1 N, 289.0 E	12-2	1200	863	1040	Jordan et al. (2009)
Durham, USA (2006-2008)	id.	3-5	2170	1952	3693	id.
Durham, USA (2004-2007)	id.	6-8	3350	4571	6657	id.
Durham, USA (2005-2007)	id.	9-11	1370	1425	2004	id.

Table S1. Continued.

Site	Coordinates	Month	Obs.	A priori	Optimised	Reference
		Europe				
Bremen Campus, Germany (2004)	53.1 N, 8.8 E	7	2200	2947	4606	Solomon et al. (2005)
Juelich, Germany (2003)	50.9 N, 6.4 E	7	8000	4140	5525	Spirig et al. (2005)
Innsbruck, Austria (1997)	47.2 N, 11.35 E	9	3000	2017	2360	Holzinger et al. (2001)
Castelporziano, Italy (2007)	41.7 N, 12.38 E	5	3510	2453	3497	Davison et al. (2009)
Northern Italy (2013)	45.8 N, 8.63 E	6	6220	4513	6305	Jensen et al. (2018)
Creta, Greece (2001)	35 N, 25.25 E	8	3500	2047	1840	de Gouw et al. (2004)
Cyprus (2014)	35 N, 32.4 E	7-8	3242	1731	1657	Derstroff et al. (2017)
Athens, Greece (2001)	38 N, 24 E	8	4500	3181	2791	de Gouw et al. (2004)
Raunefjord, Norway (2005)	60.3 N, 5.3 E	6	1860	1064	1470	Sinha et al. (2007)
Central Switzerland (2004)	47.3 N, 7.8 E	7	6000	3694	4187	Brunner et al. (2007)
Zurich, Switzerland (2005)	47.3 N, 8.5 E	4	2180	2942	5388	Legreid et al. (2007)
id.	id.	7	3180	3716	4173	id.
id.	id.	11	1110	1431	1521	id.
id.	id.	12	1210	1481	1577	id.
Jungfraujoch, Switzerland (2005)	46.5 N, 8 E	4-5	790	827	1312	Legreid et al. (2008)
id.	id.	8-9	769	794	966	id.
id.	id.	10	362	456	532	id.
id.	id.	2-3	550	358	400	id.
Montseny, Spain (2009)	41.7 N, 2.35 E	2-3	1840	832	1053	Seco et al. (2011)
id.	id.	7-8	4920	2349	1823	id.
Montseny, Spain (2019)	41.7 N, 2.35 E	7-8	4600	2800	2712	Yanez-Serrano et al. (2021)
id.	id.	9	1990	1810	1809	id.
id.	id.	10	1600	1335	1558	id.
Hyytiälä forest, Finland (2007)	61.8 N, 24.3 E	1	190	476	500	Patokoski et al. (2014)
id.	id.	4	640	887	1248	id.
		Other				
Shenzhen, China (2022)	22.6 N, 114 E	9-10	3700	4324	3005	Li et al. (2024)
Yangmeikeng, China (2016)	22.5 N, 114.6 E	6-7	3900	3411	2463	Han et al. (2019)
Seoul, South Korea (2016)	37.6 N, 127 E	5-6	11500	3908	9246	Beaudry et al. (2025)
Beijing, China (2017)	39.9 N, 116.4 E	5-6	16500	4626	17234	id.
Indian Ocean, 0-13 S (1999)	0-13 S, 71-73 E	3	600	642	635	Wisthaler et al. (2002)
Indian Ocean, 9-13 N (1999)	9-13 N, 67-70 E	3	1057	833	931	id.
Indian Ocean, 13-19 N (1999)	13-19 N, 66-70 E	3	687	716	794	id.
Indian Ocean, 7.5 N (1999)	7.5 N, 70 E	3	1417	917	968	id.
Atlantic, 1.7±1.3 km (2004)	35.8–40.2 N, 321.4–332.6 E	7-8	530	527		Lewis et al. (2007)
Atlantic, 2.4±1.4 km	36–44 N, 326–338 E	id.	630	544	659	id.
Atlantic, 3.5±1.7 km	40.5–45.5 N, 325–335 E	id.	1100	598	815	id.
Atlantic, 6.1±1.9 km	36.5–43.5 N, 323–341 E	id.	680	543	752	id.
Atlantic, 6.7±2.3 km	36.1–41.9 N, 319.8–334.2 E	id.	380	540	723	id.
Mauna Loa, Pacific (2001)	19.5 N, 204.4 E	3-4	900	627	635	Karl et al. (2003a)
Tropical Atlantic (2002)	0-10 N, 325-340 E	10-11	890	935	804	Williams et al. (2004)
Mace Head, Ireland (2002)	53.3 N, 350 E	7-9	802	729	957	Lewis et al. (2005)
Cape Verde (2006-2011)	16.9 N, 335.1 E	1-12	742	519	524	Read et al. (2012)
Maido, Reunion Isl. (2017-2019)	21.1 S, 55.4 E	1-12	961	498	513	Verreyken et al. (2021)
Wollongong, Australia (2012-2013)	34.4 S, 150.9 E	12-2	2234	1649	1718	Paton-Walsh et al. (2017)

Table S2. FTIR stations contributing in this work: longitude, latitude, altitude above sea level, microwindows, database for spectroscopy, and reference.

Station	Latitude North	Longitude East	Altitude (km)	Microwindow (cm^{-1})	Spectroscopy database	Reference
Eureka	80.05	-86.42	0.61	992.0–998.7; 1029.0–1037.0	HITRAN 2008	Viatte et al. (2014), Wizenberg et al. (2024)
St. Petersburg	59.88	29.83	0.02	992.0–998.7; 1029.0–1037.0	HITRAN 2016	Viatte et al. (2014)
Jungfraujoch	46.550	7.98	3.58	992.0–998.7; 1029.0–1037.0	HITRAN 2008	Bader et al. (2014)
Toronto	43.60	-79.40	0.17	992.0–998.7; 1029.0–1037.0	HITRAN 2008	Viatte et al. (2014), Yamanouchi et al. (2023)
Kitt Peak Obs.	31.90	-111.60	2.09	992.0–998.7	HITRAN 2004	Rinsland et al. (2009)
Porto Velho	-8.77	-63.87	0.09	1029.0–1037.0	HITRAN 2012	Vigouroux et al. (2012)
La Réunion (St. Denis)	-20.90	55.48	0.08	1029.0–1037.0	HITRAN 2012	Vigouroux et al. (2012)
La Réunion (Maïdo)	-21.08	55.38	2.16	1029.0–1037.0	HITRAN 2012	Vigouroux et al. (2012)

Table S3. Methanol dry deposition velocity measurements used in this work for evaluation. LAI is the reported leaf area index (m^2 m^{-2}), when available, v_d^{obs} and v_d^{mod} the average measured and modelled deposition velocity, respectively. PFT is the the plant functional type. Notes: *: nighttime; a: variable, provided by the MODIS dataset. References: 1, Wohlfahrt et al. (2015); 2, Schade and Goldstein (2001); 3, Karl et al. (2005); 4, Rantala et al. (2015); 5, Schade et al. (2011); 6, McKinney et al. (2011); 7, Schallhart et al. (2006); 8, Seco et al. (2015); 9, Langford et al. (2010); 10, Misztal et al. (2011); 11, Holst et al. (2010); 12, Brunner et al. (2007); 13, Hörtnagl et al. (2011).

Site	**Dominant PFT**	**Coordinates**	**Month(s)/year(s)**	**LAI**	v_d^{obs} (v_d^{mod})	**Reference**
Blodgett, USA	pine plantation	38.8 N, 239.3 E	6-7/1999	1.5	1.8* (1.45)	1, 2
Duke forest, USA	pine plantation	35.98 N, 280.9 E	7/2003	3	0.96* (0.86)	3
Vielsalm, Belgium	mostly coniferous	50.3 N, 5.99 E	3-11/2009-11	3.5	1.9* (1.52)	1
Hyytiälä, Finland	coniferous	61.8 N, 24.3 E	5-9/2010-13	6	0.29 (1.34)	4
Soroe, Denmark	beech forest	55.4 N, 11.7 E	6/2007	5	1.1 (0.75)	5
Harvard forest, USA	mixed forest	42.54 N, 287.83 E	6-7/2007	5	1.0* (0.72)	1, 6
Bosco Fontana, Italy	oak forest	45.2 N, 10.74 E	6-8/2012	3.5	0.21* (0.22)	7
Ozarks, USA	deciduous	38.76 N, 267.84 E	5-10/2012	a	0.3* (0.44)	1, 8
Bukit Atur, Borneo	rainforest	4.9 N, 117.8 E	4-7/2008	6	0.47 (0.76)	9
Borneo plantation	palm trees	5.2 N, 118.4 E	5-6/2008	6	1.25 (0.76)	10
Stordalen, Sweden	wetland	68.33 N, 19.05 E	5-9/2007	a	0.70* (0.42)	1, 11
Oesingen, Switzerland	grassland	47.28 N, 7.73 E	6-7/2004	a	0.15* (0.14)	1, 12
Neustift, Austria	grassland	47.12 N, 11.32 E	3-11/2008-12	a	0.50* (0.46)	13
Average over all sites					*0.82 (0.76)*	

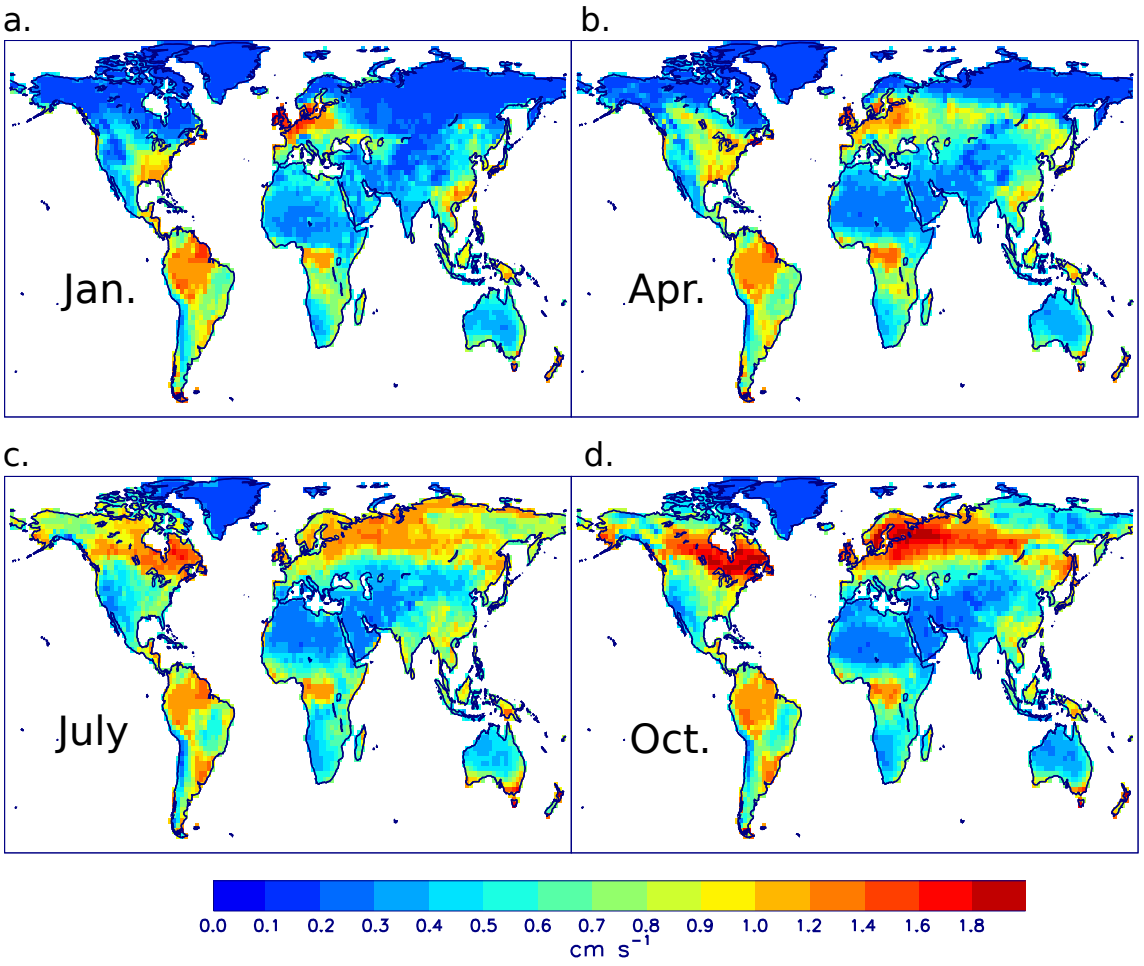

Figure S3. Climatological (2008–2019) monthly methanol dry deposition velocities at $2^\circ \times 2.5^\circ$ ($\mathrm{cm\,s^{-1}}$) over land areas, for (a) January, (b) April, (c) July and (d) October.

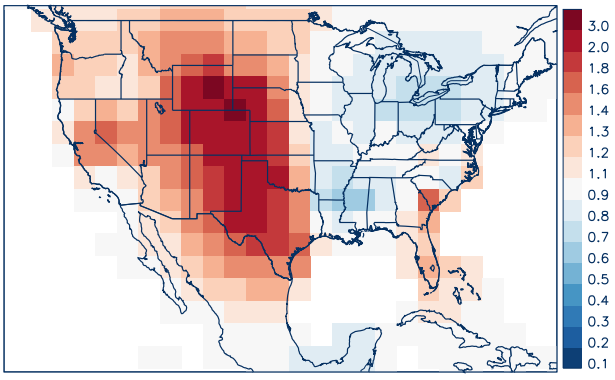

Figure S4. Enhancement of summertime biogenic emissions (May–September 2012–2013 average), relative to the a priori inventory, obtained in the aircraft-based optimisation.

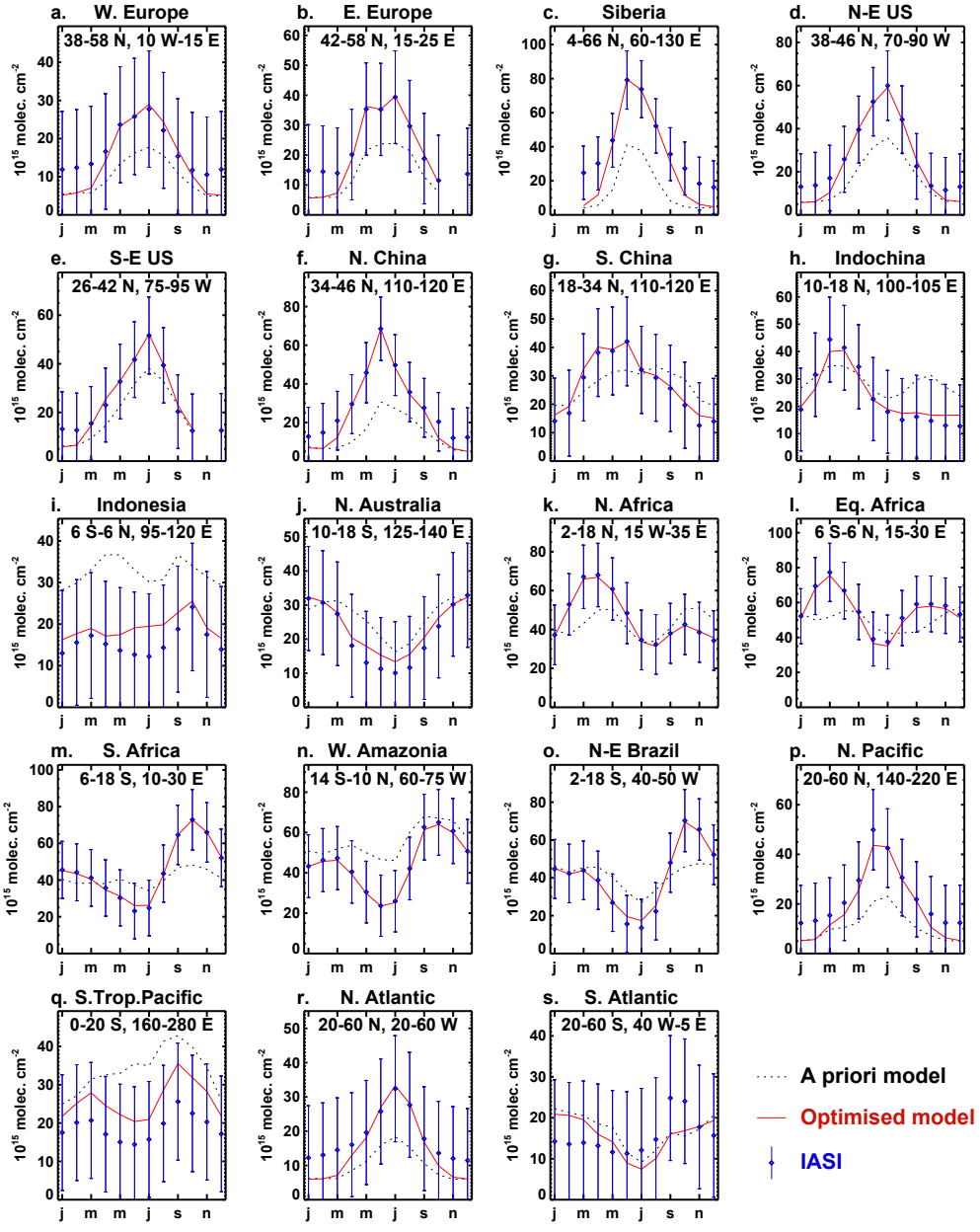

Figure S5. Seasonal variation (2008–2019 average) of CH_3OH columns (10^{15} molec.cm^{-2}) over large regions. Symbols: bias-corrected IASI; dotted line: model with a priori emissions; red line: and optimised emissions (red line). Error bars denote the combined observational and model error adopted in the emission inversion.

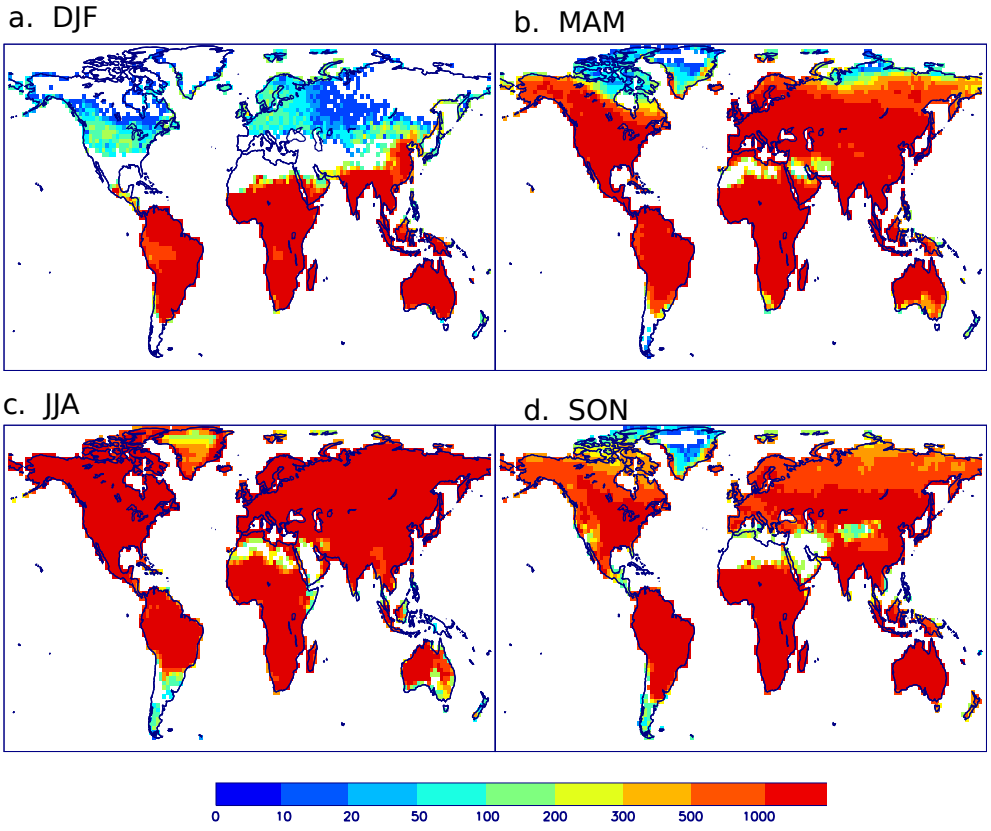

Figure S6. Average number of IASI measurements per pixel and per season used in the emission optimisations, on average between 2008 and 2019.

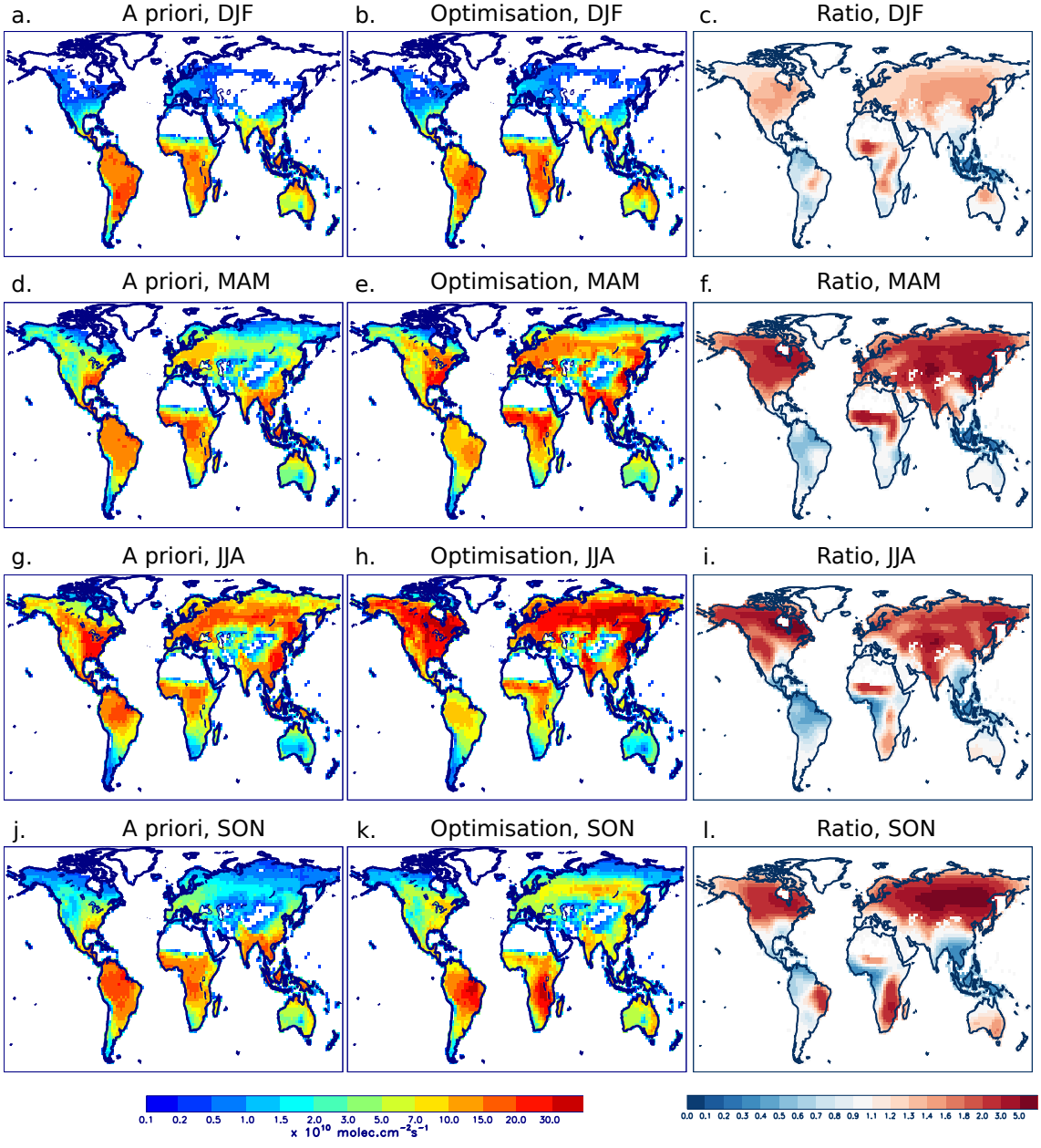

Figure S7. Seasonally-averaged biogenic emissions (2008-2019 averages in 10^{10} molec.cm^{-2} s^{-1}) in the a priori simulation (left panels) and in the optimisation (middle panels). The ratio of optimised to priori emissions is displayed on the right panels..)

Table S4. Statistics of comparison of in situ CH_3OH measurements from aircraft campaigns with model runs using either a priori emissions or emissions constrained by IASI. n is the number of measurements. The bias is calculated as $100 \cdot (< C_m - C_o >) / < C_o >$, with C_m and C_o the modelled and observed mixing ratios, respectively, and <> denote the average over all data from each campaign. The root-mean-square deviation (RMSD) is calculated as $(< (C_m - C_o)^2 >)^{1/2}$. Only data below 8 km altitude are considered. Data over ocean are excluded from all campaigns except ATom. See main manuscript for additional details on the campaigns.

	n	C_o (ppbv)	Bias A priori (%)	Bias Optimised (%)	RMSD A priori (ppbv)	RMSD Optimised (ppbv)
ARCTAS June (PTR-MS)	1612	2.67	-36	-15	1.23	0.74
ARCTAS June (TOGA)	1369	2.23	-24	2	0.83	0.60
ARCTAS July (PTR-MS)	1773	2.67	-24	49	0.93	2.11
ARCTAS July (TOGA)	1463	2.89	-23	51	1.47	2.80
DC3 (DC8)	2847	3.19	-45	-29	1.66	1.15
DC3 (GV)	2055	3.28	-50	-34	1.83	1.30
SENEX	6273	5.29	-23	-22	1.26	1.23
SEAC^{4}RS	4732	2.85	0	-3	0.50	0.26
GoAmazon	1765	1.55	32	1	0.71	0.36
KORUS-AQ	1057	6.08	-77	-45	5.07	2.84
All campaigns over land	*24946*	*3.52*	*-22.7*	*-8.4*	*1.29*	*1.14*
			Over ocean			
ATom 1-4	3510	0.60	-21	-15	0.163	0.130

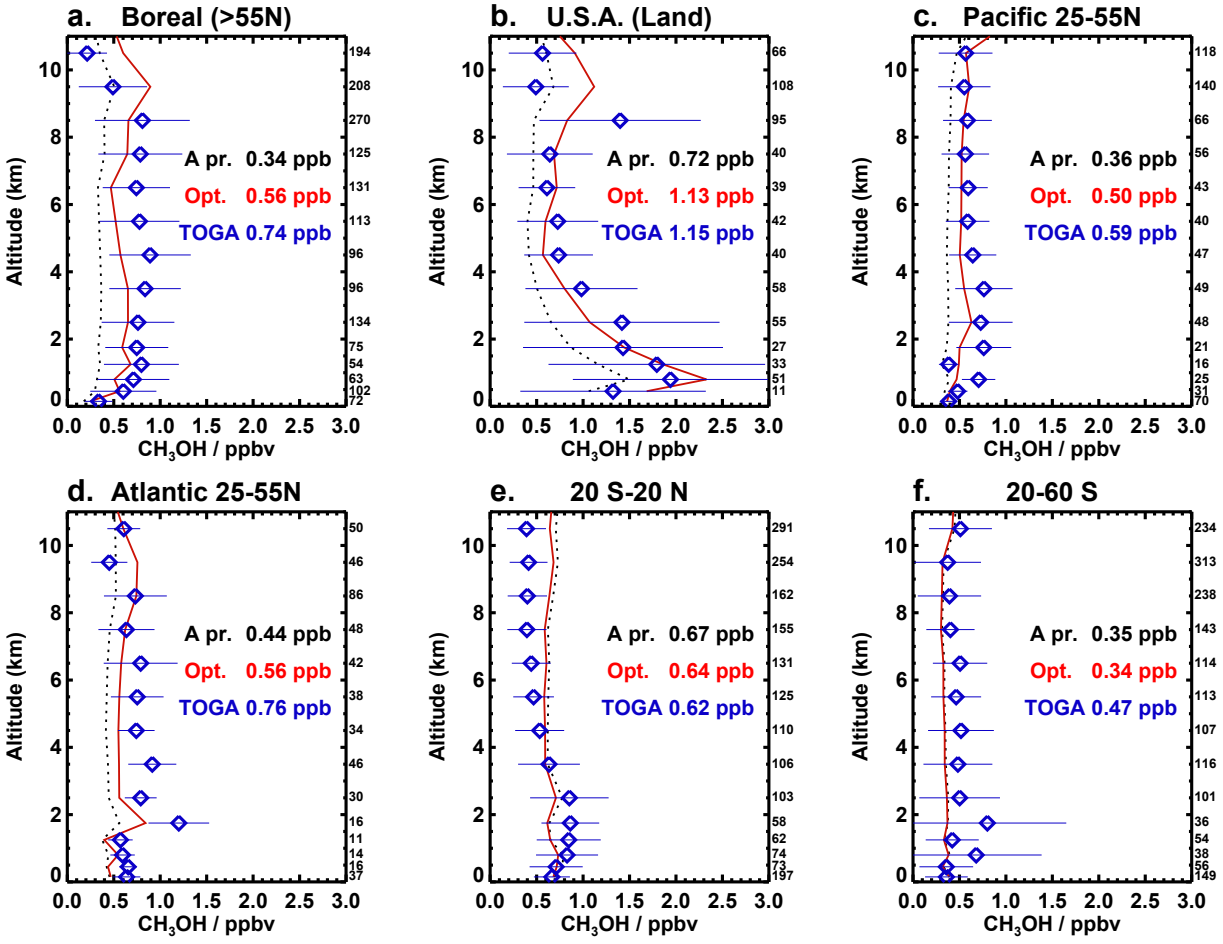

Figure S8. Averaged vertical profiles of observed CH_3OH concentrations (symbols) from the ATom campaigns (Fig. 2 and Table 2 of main manuscript) (a) poleward of 55°N, (b) over contiguous U.S., (c) N. Pacific (25–55°N), (d) N. Atlantic (25–55°N), (e) tropical oceans (20°–20°N), and (f) southern oceans (20°S–60°S). Dotted lines: prior model profiles; red lines: IASI-based optimisation. The error bars denote the standard deviation of the observations. The number of observations per altitude bin is indicated on the right of each plot. The average observed and modelled mixing ratios below 8 km altitude are given for each region. Data over land are excluded for all regions except for panels a and b.

Table S5. Summary of comparison between in situ CH_3OH mixing ratio measurements and corresponding model values (in pppv) before and after IASI-based emission optimisation, averaged over large regions. The measurement sites are detailed in Table S1.

	Number of campaigns	Observed (ppbv)	A priori model (ppbv)	Optimisation (ppbv)	Ratio optimised/observed
Tropical forests	10	1.77	2.76	2.03	1.15
U.S.A.	14	2.63	2.18	3.09	1.17
Europe	25	1.92	1.62	1.90	0.99
East Asia	4	7.23	4.04	5.86	0.81
Marine	14	0.77	0.64	0.72	0.93
All	67	2.12	1.85	2.16	1.02

Table S6. Statistics of the comparison between FTIR CH_3OH column measurements and model simulations using either a priori or top-down emissions. n is the number of measurements. The bias (%) is calculated as $100 \cdot (< C_m - C_o >) / < C_o >$, where C_m and C_o denote the mean modelled and observed monthly columns, respectively, and <> denote the average over all data from each station. The root-mean-square deviation (RMSD) is calculated as $(< (C_m - C_o)^2 >)^{1/2}$. R denotes Pearson's correlation coefficient. For Porto Velho, the statistics are for the alternative optimisation ignoring IASI data between 13 and 30 September, 2019 (see text).

		C_o	Bias (%)		RMSD (10^{15}cm^{-2})		R	
	n	(10^{15}cm^{-2})	A priori	Optimised	A priori	Optimised	A priori	Optimised
Eureka (2008–2019)	1920	20.8	-70	-40	14.9	8.9	0.74	0.78
Toronto (2008–2019)	1148	37.2	-25	12	10.4	8.8	0.90	0.88
St Petersburg (2009–2019)	4861	21.0	-20	21	6.4	9.1	0.89	0.92
Jungfraujoch (2008–2019)	2574	7.2	-30	-6	3.2	1.7	0.82	0.90
St Denis, Reunion (2009–2011)	1312	12.0	5	4	2.6	1.6	0.45	0.86
Maïdo, Reunion (2013–2019)	4346	9.3	13	11	2.8	1.9	0.36	0.82
Porto Velho (June–Oct. 2019)	568	42.5	35	24	15.4	14.8	1.00	0.95
Kitt Peak (1985–2003)	86	9.6	-22	-12	3.3	1.9	0.87	0.96

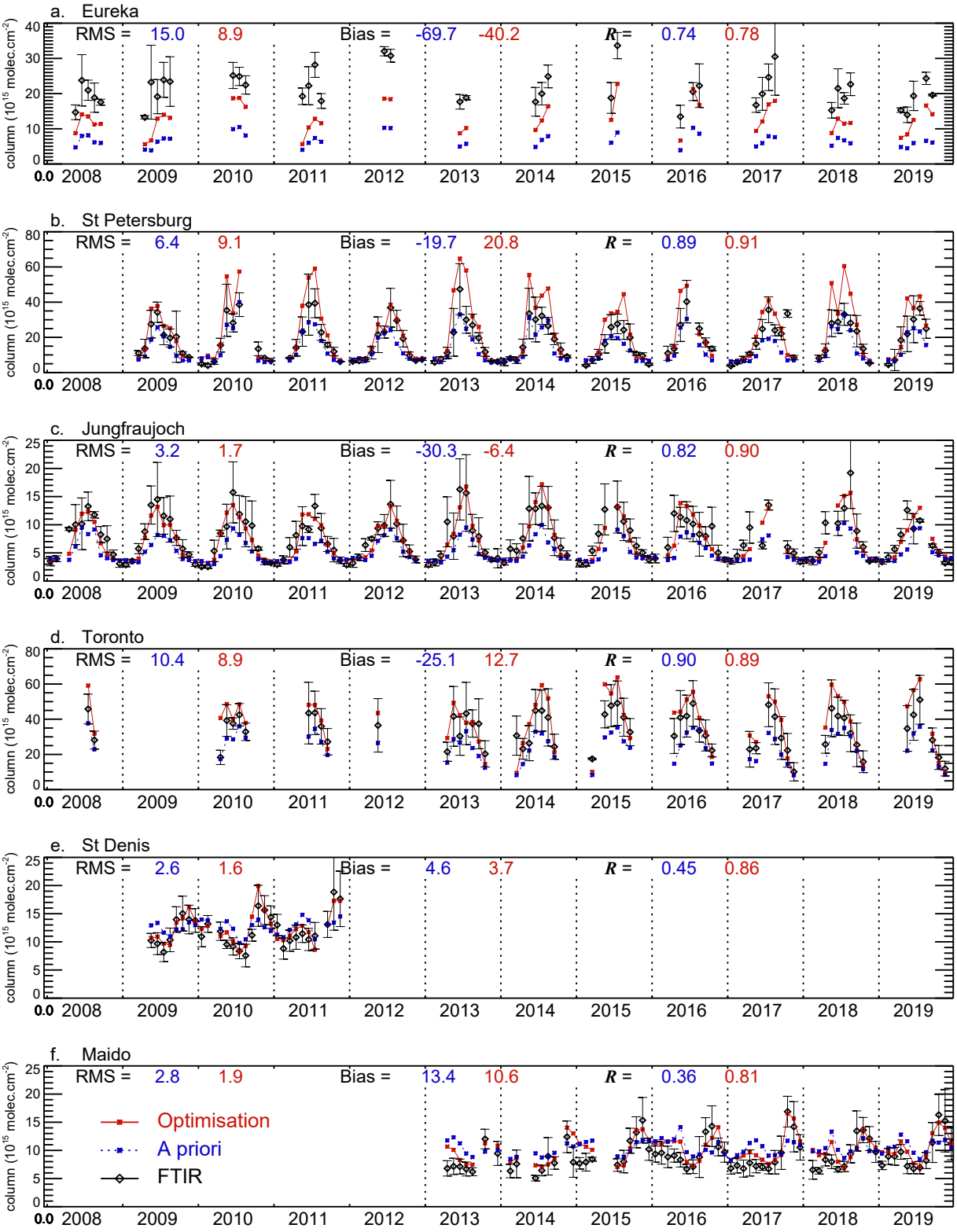

Figure S9. Time series of monthly averaged FTIR CH_3OH columns (black symbols) between 2008 and 2019, and corresponding model values from the a priori run (dotted dark blue lines) and optimised run (red lines), respectively. The model averages are calculated using the FTIR averaging kernels and model vertical profiles at the FTIR sampling times. Months for which the number of FTIR measurements is lower than three are excluded. The root mean squared deviation (RMS) and absolute bias (10^{15} molec.cm^{-2}), as well as Pearson's coefficient of correlation (R) are also given. The error bars denote the standard deviation of the monthly averaged data.

Table S7. Plant functional types (PFT) and values of parameters involved in the dry deposition scheme. All resistance units are s m^{-1}.

Plant functional types	a_s J m^{-3}	b_s J m^{-2}	c_s	d_s hPa^{-1}	R_{ac0}^{min}	R_{ac0}^{max}	$R_{cutd0}^{O_3}$	$R_{cutw0}^{O_3}$	$R_{cut}^{SO_2}$	$R_{gd}^{SO_2}$
Needleleaf evergreen trees	14000	2	18	0.031	100	100	6000	300	2000	200
Needleleaf deciduous trees	14000	2	18	0.031	60	100	6000	300	2000	200
Broadleaf evergreen trees	4000	6	20	0.036	250	250	9000	600	2500	100
Broadleaf deciduous trees	10000	5	30	0.036	100	250	9000	600	2500	200
Shrub	10000	5	30	0.031	60	60	7500	450	2000	200
Crop	20000	6	90	0.0	10	40	6000	300	1500	200
Grass	5000	1	50	0.024	10	40	6000	300	1000	200

References

Bader, W., Stavrakou, T., Müller, J.-F., Reimann, S., Boone, C. D., Harrisson, J. J., Flock, O., Bovy, B., Franco, B., Lejeune, B., Servais, C., and Mahieu, E.: Long-term evolution and seasonal modulation of methanol above Jungfraujoch (46.5° N, 8.0° E): optimisation of the retrieval strategy, comparison with model simulations and independent observations, Atmos. Meas. Tech., 7, 3861-3872, https://doi.org/10.5194/amt-7-3861-2014, 2014.

Beaudry, E., D. J. Jacob, K. H. Bates, S. Zhai, L. H. Yang, D. C. Pendergrass, N. Colombi, I. J. Simpson, A. Wisthaler, J. R. Hopkins, K. Li, and H. Liao: Ethanol and methanol in South Korea and China: Evidence for large anthropogenic emissions missing from current inventories, ACS ES&T Air, 2, 456–465, https://doi.org/10.1021/acsestair.4c00210, 2025.

Brunner, A., Ammann, C., Neftel, A., and Spirig, C.: Methanol exchange between grassland and the atmosphere, Biogeosciences, 4, 395–410, https://doi.org/10.5194/bg-4-395-2007, 2007.

Davison, B., Taipale, R., Langford, B., Misztal, P., Fares, S., Matteucci, G., Loreto, F., Cape, J. N., Rinne, J., and Hewitt, C. N.: Concentrations and fluxes of biogenic volatile organic compounds above a Mediterranean macchia ecosystem in western Italy, Biogeosciences, 6, 1655–1670, https://doi.org/10.5194/bg-6-1655-2009, 2009.

de Gouw, J., Warneke, C., Holzinger, R., Klupfel, T., and Williams, J.: Inter-comparison between airborne measurements of methanol, acetonitrile and acetone using two differently configured PTR-MS instruments, Int. J. Mass Spectr., 239, 129–137, 2004.

Derstroff, B., Hüser, I., Bourtsoukidis, E., Crowley, J. N., Fischer, H., Gromov, S., Harder, H., Janssen, R. H. H., Kesselmeier, J., Lelieveld, J., Mallik, C., Martinez, M., Novelli, A., Parchatka, U., Phillips, G. J., Sander, R., Sauvage, C., Schuladen, J., Stönner, C., Tomsche, L., and Williams, J.: Volatile organic compounds (VOCs) in photochemically aged air from the eastern and western Mediterranean, Atmos. Chem. Phys., 17, 9547–9566, https://doi.org/10.5194/acp-17-9547-2017, 2017.

Han, Y., Huang, X., Wang, C., Zhu, B., and He, L.: Characterizing oxygenated volatile organic compounds and their sources in rural atmospheres in China, J. Environ. Sci., 81, 148-155, https://doi.org/10.1016/j.jes.2019.01.017, 2019.

Holst, T., Arneth, A., Hayward, S., Ekberg, A., Mastepanov, M., Jackowicz-Korczynski, M., Friborg, T., Crill, P. M., and Bäckstrand, K.: BVOC ecosystem flux measurements at a high latitude wetland site, Atmos. Chem. Phys., 10, 1617–1634, doi:10.5194/acp-10-1617-2010, 2010.

Holzinger, R., Jordan, A., Hansel, A., and Lindinger, W.: Methanol measurements in the lower troposphere near Innsbruck (47°16′N; 11°24′E), Austria, Atmos. Environ., 35, 2525–2532, 2001.

Hörtnagl, L., Bamberger, I., Graus, M., Ruuskanen, T. M., Schnitzhofer, R., Müller, M., Hansel, A., Wohlfahrt, G.: Biotic, abiotic, and management controls on methanol exchange above a temperate mountain grassland, J. Geophys. Res., 116 (G3), https://doi.org/10.1029/2011JG001641, 2011.

Jensen, N. R., Gruening, C., Goded, I., Müller, M., Hjorth, J., and Wisthaler, A.: Eddy-covariance flux measurements in an Italian deciduous forest using PTR-ToF-MS, PTR-QMS and FIS, Int. J. Environ. Anal. Chem., 98(8), 758–788, https://doi.org/10.1080/03067319.2018.1502758, 2018.

Jordan, C., Fitz, E., Hagan, T., Sive, B., Frinak, E., Haase, K., Cottrell, L., Buckley, S., and Talbot, R.: Long-term study of VOCs measured with PTR-MS at a rural site in New Hampshire with urban influences, Atmos. Chem. Phys., 9, 4677–4697, https://doi.org/10.5194/acp-9-4677-2009, 2009.

Karl, T., Guenther, A., Spirig, C. Hansel, A., and Fall, R.: Seasonal variation of biogenic VOC emissions above a mixed hardwood in northern Michigan, Geophys. Res. Lett., 30, 2186, doi:10.1029/2003GL018432, 2003a.

Karl, T., Hansel, A., Märk, T., Lindinger, W., and Hoffmann, D.: Trace gas monitoring at the Mauna Loa Baseline Observatory using Proton-Transfer Reaction Mass Spectrometry, Int. J. Mass. Spec., 223–224, 527–538, 2003b.

Karl, T., Potosnak, M., Guenther, A., Clark, D., Walker, J., Herrick, J. D., and Geron, C.: Exchange processes of volatile organic compounds above a tropical rain forest: Implications for modelling troposheric chemistry above dense vegetation, J. Geophys. Res., 109, D18306, doi:10.1029/2004JD004738, 2004.

Karl, T., Harley, P., Guenther, A., Rasmussen, R., Baker, B., Jardine, K., and Nemitz, E.: The bi-directional exchange of oxygenated VOCs between a loblolly pine (Pinus taeda) plantation and the atmosphere, Atmos. Chem. Phys., 5, 3015–3031, doi:10.5194/acp-5-3015-2005, 2005.

Karl, T., Guenther, A., Yokelson, R. J., Greenberg, J., Potosnak, M., Blake, D. R., and Artaxo, P.: The tropical forest and fire emissions experiment, Emission, chemistry, and transport of biogenic volatile organic compounds in the lower atmosphere over Amazonia, J. Geophys. Res., 112, D18302, doi:10.1029/2007JD008539, 2007.

Kesselmeier, J., P. Ciccioli, U. Kuhn, P. Stefani, T. Biesenthal, S. Rottenberger, Wolf, A., Vitullo, M., Nobre, A., Kabat, P., and Andreae, M. O.: Volatile organic compound emissions in relation to plant carbon fixation and the terrestrial carbon budget, Global Biogeochem. Cy., 16, https://doi.org/10.1029/2001GB001813, 2002.

Langford, , Misztal, P. K., Nemitz, E., Davison, B., Helfter, C., Pugh, T. A. M., MacKenzie, A. R., Lim, S. F., and Hewitt, C. N: Fluxes and concentrations of volatile organic compounds from a South-East Asian tropical rainforest, Atmos. Chem. Phys., 10, 8391–8412, doi:10.5194/acp-10-8391-2010, 2010.

Lewis, A. C., Hopkins, J. R., Carpenter, L. J., Stanton, J., Read, K. A., and Pilling, M. J.: Sources and sinks of acetone, methanol, and acetaldehyde in North Atlantic marine air, Atmos. Chem. Phys., 5, 1963–1974, https://doi.org/10.5194/acp-5-1963-2005, 2005.

Lewis, A. C., Evans, M. J., Methven, J., Watson, N., Lee, J. D., Hopkins, J. R., Purvis, R. M., Arnold, S. R., McQuaid, J. B., Whalley, L. K., Pilling, M. J., Heard, D. E., Monks, P. S., Parker, A. E., Reeves, C. E., Oram, D. E., Mills, G., Bandy, B. J., Stewart, D., Coe, H., Williams,

P., Crosier, J.: Chemical composition observed over the mid-Atlantic and the detection of pollution signatures far from source regions, J. Geophys. Res., 112, D10S39, doi:10.1029/2006JD007584, 2007.

Zhi-Jie Li, Z.-L., He, L.-Y., Ma, H.-N., Peng, X., Tang, M.-X., Du, K., and Huang, X.-F.: Sources of atmospheric oxygenated volatile organic compounds in different air masses in Shenzhen, China, Environ. Poll., 340, 122871, https://doi.org/10.1016/j.envpol.2023.122871, 2024.

Legreid, G., Balzani Lööv, J., Staehelin, J., Hueglin, C., Hill, M., Buchmann, B., Prevot, A. S. H., and Reimann, S.: Oxygenated volatile organic compounds (OVOCs) at an urban background site in Zürich (Europe): Seasonal variation and source allocation, Atmos. Environ., 41, 8409–8423, https://doi.org/10.1016/j.atmosenv.2007.07.026, 2007.

Legreid, G., Folini, D., Staehelin, J., Lööv, J. B., Steinbacher, M. and Reimann, S.: Measurements of organic trace gases including oxygenated volatile organic compounds at the high alpine site Jungfraujoch (Switzerland): Seasonal variation and source allocations, J. Geophys. Res. 113 (D5), https://doi.org/10.1029/2007JD008653, 2008.

Lelieveld, J., Butler, T., Crowley, J., Dillon, T. J., Fischer, H., Ganzeveld, L., Harder , H., Lawrence, M. G., Martinez, M., Taraborrelli, D., and Williams, J.: Atmospheric oxidation capacity sustained by a tropical forest, Nature, 452, 737–740, https://doi.org/10.1038/nature06870, 2008.

Mao, H., Talbot, R., Nielsen, C., and Sive, B.: Controls on methanol and acetone in marine and continental atmospheres, Geophys. Res. Lett., 33, L02803, doi:10.1029/2005GL024810, 2006.

McKinney, K. A., Lee, B. H., Vasta, A., Pho, T. V., and Munger, J. W.: Emissions of isoprenoids and oxygenated biogenic volatile organic compounds from a New England mixed forest, Atmos. Chem. Phys., 11, 4807–4831, https://doi.org/10.5194/acp-11-4807-2011, 2011.

Millet, D. B., Goldstein, A. H., Holzinger, R., Allan, J. D., Jimenez, J. L., Worsnop, D. R., Roberts, J. M., White, A. B., Hudman, R. C., Bertschi, I. T., Stohl, A.: Chemical characteristics of North American surface layer outflow: Insights from Chebogue Point, Nova Scotia, J. Geophys. Res., 111, D23S53, https://doi.org/10.1029/2006JD007287, 2006.

Misztal, P., Nemitz, E., Langford, B., Di Marco, C. F., Phillips, G. J., Hewitt, C. N., MacKenzie, A. R., Owen, S. M., Fowler, D., Heal, M. R., and Cape, J. N.: Direct ecosystem fluxes of volatile organic compounds from oil palms in South-East Asia, Atmos. Chem. Phys., 11, 8995–9017, doi:10.5194/acp-11-8995-2011, 2011.

Patokoski, J., Ruuskanen, T. M., Hellén, H., Taipale, R., Grönholm, T., Kajos, M. J., Petäjä, T., Hakola, H., Kulmala, M., and Rinne, J.: Winter to spring transition and diurnal variation of VOCs in Finland at an urban background site and a rural site, Bor. Environ. Res., 19, 79-103, https://doi.org/10.60910/79ew-2erz, 2014.

Paton-Walsh, C., Guérette, É.-A., Kubistin, D., Humphries, R., Wilson, S. R., Dominick, D., Galbally, I., Buchholz, R., Bhujel, M., Chambers, S., Cheng, M., Cope, M., Davy, P., Emmerson, K., Griffith, D. W. T., Griffiths, A., Keywood, M., Lawson, S., Molloy, S., Rea, G., Selleck, P., Shi, X., Simmons, J., and Velazco, V.: The MUMBA campaign: measurements of urban, marine and biogenic air, Earth Syst. Sci. Data, 9, 349–362, https://doi.org/10.5194/essd-9-349-2017, 2017.

Rantala, P., Aalto, J., Taipale, R., Ruuskanen, T., and Rinne, J.: Annual cycle of volatile organic compound exchange between a boreal pine forest and the atmosphere, Biogeosciences, 12, 5723–5770, doi:10.5194/bg-12-5753-2015, 2015.

Read, K. A., Carpenter, L. J., Arnold, S. R., Beale, R., Nightingale, P. D., Hopkins, J. R., Lewis, A. C., Lee, J. D., Mendes, L., and Pickering, S. J.: Multiannual observations of acetone, methanol, and acetaldehyde in remote tropical Atlantic air: Implications for atmospheric OVOC budgets and oxidative capacity, Environ. Sci. Technol., 46, 20, 11028–11039, https://doi.org/10.1021/es302082p, 2012.

Rinsland, C. P., Mahieu, E., Chiou, L., and Herbin, H.: First ground-based infrared solar absorption measurements of free tropospheric methanol (CH_3OH): Multidecade infrared time series from Kitt Peak (31.9°N 111.6°W): Trend, seasonal cycle, and comparison with previous measurements, J. Geophys. Res., 114, D04309, https://doi.org/10.1029/2008JD011003, 2009.

Sanhueza, E., Holzinger, R., Donoso, L., Santana, M., Fernandez, E., and Romero, J.: Compuestos organicos volantiles en la atmosfera Gran Sabana, concentraciones y quimica atmosferica, Interciencia, 26, 597–605, 2001.

Schade, G. W. and Goldstein, A. H.: Fluxes of oxygenated volatile organic compounds from a ponderosa pine plantation, J. Geophys. Res., 106(D3), 3111–3123, https://doi.org/10.1029/2000JD900592, 2001.

Schade, G. W. and Goldstein, A. H.: Seasonal measurements of acetone and methanol: abundances and implications for atmospheric budgets, Global Biogeochem. Cy., 20, GB1011, https://doi.org/10.1029/2005GB002566, 2006.

Schade, G. W., Solomon, S. J., Dellwik, E., Pilegaard, K., and Ladstätter-Weissenmayer, A.: Methanol and other VOC fluxes from a Danish beech forest during late springtime, Biogeochemistry, 106, 337–335, https://doi.org/10.1007/s10533-010-9515-5, 2011.

Schallhart, S., Rantala, P., Nemitz, E., Taipale, D., Tillmann, R., Mentel, T. F., Loubet, B., Gerosa, G., Finco, A., Rinne, J., and Ruuskanen, T. M.: Characterization of total ecosystem-scale biogenic VOC exchange at a Mediterranean oak-hornbeam forest, Atmos. Chem. Phys., 16, 7171–7194, doi:10.5194/acp-16-7171-2016, 2016.

Seco, R., Peñuelas, J., Filella, I., Llusià, J., Molowny-Horas, R., Schallhart, S., Metzger, A., Müller, M., and Hansel, A.: Contrasting winter and summer VOC mixing ratios at a forest site in the Western Mediterranean Basin: the effect of local biogenic emissions, Atmos. Chem. Phys., 11, 13161–13179, https://doi.org/10.5194/acp-11-13161-2011, 2011.

Seco, R., et al.: GOAMAZON 2014/15 campaign: SRI-PTR-TOF-MS VOC data from the T3 site in Manacapuru (Amazonas, Brasil). Dataset available at : https://adc.arm.gov/discovery/#/results/id::6653_voc_microchem_ptrms_aerosol_voc

Seco, R., Karl, T., Guenther, A., Hosman, K. P., Pallardy, S. P., Gu, L., Geron, C., Harley, P., and Kim, S.: Ecosystem-scale volatile organic compound fluxes during an extreme drought in a broadleaf temperate forest of the Missouri Ozarks (central USA), Glob. Chang. Biol., 21 (10), 3657-3674, https://doi.org/10.1111/gcb.12980, 2015.

Sinha, V., Williams, J., Meyerhöofer, M., Riebesell, U., Paulino, A. I., and Larsen, A.: Air-sea fluxes of methanol, acetone, acetaldehyde, isoprene and DMS from a Norwegian fjord following a phytoplankton bloom in a mesocosm experiment, Atmos. Chem. Phys., 7, 739–755, doi:10.5194/acp-7-739-2007, 2007.

Solomon, S. J., Custer, T., Schade, G., Soares Dias, A. P., and Burrows, J.: Atmospheric methanol measurement using selective catalytic methanol to formaldehyde conversion, Atmos. Chem. Phys., 5, 2787–2796, doi:10.5194/acp-5-2787-2005, 2005.

Spirig, C., Neftel, A., Ammann, C., Dommen, J., Grabmer, W., Thielmann, A., Schaub, A., Beauchamp, J., Wisthaler, A., and Hansel, A.: Eddy covariance flux measurements of biogenic VOCs during ECHO 2003 using proton transfer reaction mass spectrometry, Atmos. Chem. Phys., 5, 465–481, https://doi.org/10.5194/acp-5-465-2005, 2005.

Verreyken, B., Amelynck, C., Schoon, N., Müller, J.-F., Brioude, J., Kumps, N., Hermans, C., Metzger, J.-M., Colomb, A., and Stavrakou, T.: Measurement report: Source apportionment of volatile organic compounds at the remote high-altitude Maïdo observatory, Atmos. Chem. Phys., 21, 12965–12988, https://doi.org/10.5194/acp-21-12965-2021, 2021.

Viatte, C., Strong, K., Walker, K. A., and Drummond, J. R.: Five years of CO, HCN, C_2H_6, C_2H_2, CH_3OH, HCOOH and H_2CO total columns measured in the Canadian high Arctic, Atmos. Meas. Tech., 7, 1547–1570, https://doi.org/10.5194/amt-7-1547-2014, 2014.

Vigouroux, C., Stavrakou, T., Whaley, C., Dils, B., Duflot, V., Hermans, C., Kumps, N., Metzger, J.-M., Scolas, F., Vanhaelewyn, G., Müller, J.-F., Jones, D. B. A., Li, Q., and De Mazière, M.: FTIR time-series of biomass burning products (HCN, C_2H_6 , C_2H_2 , CH_3OH, and HCOOH) at Reunion Island (21° S, 55° E) and comparisons with model data, Atmos. Chem. Phys., 12, 10367–10385, https://doi.org/10.5194/acp-12-10367-2012, 2012.

Williams, J., Pöschl, U., Crutzen, P. J., Hansel, A., Holzinger, R., Warneke, C., Lindinger, W., and Lelieveld, J.: An atmospheric Chemistry interpretation of mass scans obtained from a proton transfer mass spectrometer flown over the tropical rainforest of Suriname, J. Atmos. Chem., 38, 133–166, 2001.

Williams, J., R. Holzinger, V. Gros, X. Xu, E. Atlas, and D. W. R. Wallace: Measurements of organic species in air and seawater from the tropical Atlantic, Geophys. Res. Lett. 31, https://doi.org/10.1029/2004GL020012, 2004.

Wisthaler, A., Hansel, A., Dickerson, R. R., and Crutzen, P. J.: Organic trace gas measurements by PTR-MS during INDOEX 1999, J. Geophys. Res., 107(D19), 8024, doi:10.1029/2001JD000576, 2002.

Wizenberg, T., Strong, K., Jones, D. B. A., Hannigan, J. W., Ortega, I., and Mahieu, E.: Measured and modeled trends of seven tropospheric pollutants in the high Arctic from 1999 to 2022, J. Geophys. Res., 129, e2023JD040544, https://doi.org/10.1029/2023JD040544, 2024.

Wohlfahrt, G., Amelynck, C., Ammann, C., Arneth, A., Bamberger, I., Goldstein, A. H., Gu, L., Guenther, A., Hansel, A., Heinesch, B., Holst, T., H"ortnagel, L., Karl, T., Laffineur, Q., Neftel, A., McKineey, K., Munger, J. W., Pallardy, S. G., Schade, G. W., Seco, R., and Schoon, N.: An ecosystem-scale perspective of the net land methanol flux: synthesis of micrometeorological flux measurements, Atmos.Chem. Phys., 15, 7413–7427, https://doi.org/10.5194/acp-15-7413-2015, 2015.

Yamanouchi, S., Strong, K., Lutsch, E., and Jones, D. B. A.: Detection of HCOOH, CH_3OH, CO, HCN, and C_2H_6 in wildfire plumes transported over Toronto using ground-based FTIR measurements from 2002–2018, J. Geophys. Res., 125, e2019JD031924. https://doi.org/10.1029/2019JD031924, 2020.

Yamanouchi, S., Conway, S., Strong, K., Colebatch, O., Lutsch, E., Roche, S., Taylor, J., Whaley, C. H., and Wiacek, A.: Network for the Detection of Atmospheric Composition Change (NDACC) Fourier transform infrared (FTIR) trace gas measurements at the University of Toronto Atmospheric Observatory from 2002 to 2020, Earth Syst. Sci. Data, 15, 3387–3418, https://doi.org/10.5194/essd-15-3387-2023, 2023.

Yáñez-Serrano, A. M., Bach, A., Bartolomé-Català, Matthaios, V., Seco, R., Llusià, J., Filella, I., Peñuelas, J.: Dynamics of volatile organic compounds in a western Mediterranean oak forest, Atmos. Environ. 257, 118447, https://doi.org/10.1016/j.atmosenv.2021.118447, 2021.